

Quantifying profile stiffness

B.Ph. VAN MILLIGEN¹, R. SÁNCHEZ², V. TRIBALDOS¹, and V.I. VARGAS¹

¹Asociación EURATOM-CIEMAT para Fusión, Avda. Complutense 22, 28040 Madrid, Spain

²Fusion Energy Division, Oak Ridge National Laboratory, P.O. Box 2001, Oak Ridge, TN 37831-2001, USA

October 10, 2007

Profile stiffness is quantified using a simple technique. The approach is tested on a paradigmatic numerical stiff transport model for one field (particles). The stiffness is found to exhibit radial structure and to depend on collisionality, which might help explaining the observed lack of stiffness in stellarators, as compared to tokamaks. The extension of the approach to heat transport requires some care. A proposal for a stiffness quantifier for heat transport is made, and it is tested on data from the TJ-II stellarator.

Keywords: profile stiffness, anomalous transport, critical gradient, tokamak-stellarator comparison

DOI: 10.1585/pfr.1.001

Profile stiffness (also known as profile consistency or resilience) is the striking phenomenon that temperature or pressure profiles tend to adopt the same shape, regardless of the applied drive, at least in a certain parameter range. The phenomenon is well-established for tokamaks, but elusive in stellarators [1]. This is slightly enigmatic, since (a) power degradation is a universal phenomenon in stellarators, with a similar power dependence as in tokamaks [2] and (b) it is believed that threshold-triggered instabilities (leading to enhanced transport) should be operative both in tokamaks and stellarators. This leads to the expectation that profile stiffness should also be present in stellarators, if to a less degree (and less obviously) than in tokamaks.

The detection of profile stiffness based on the direct comparison of profiles does not allow a quantification of the degree of stiffness, while the full 1-D modelling of transport requires making assumptions not related to the stiffness issue. Therefore, a stiffness quantifier is needed to resolve this issue. In the present work we apply a standard quantifier for profile stiffness to a paradigmatic stiff particle transport model. We then discuss the possible (non-standard) extension of the method to heat transport and present first results for the TJ-II stellarator.

Profile stiffness can be understood as the sub-linear response of profile amplitudes to a (small) change in drive. Pure diffusive transport models with fixed parameters produce a proportional response of profiles to changes in fuelling or heating, since the diffusion equation is linear in the profile amplitude and the source strength. Thus, the search for profile stiffness is closely related to the study of the dependence of transport coefficients on (gradients of) the transported quantity, since such a dependence would break the linearity of the diffusion equation.

Such studies have been undertaken before [3], in the framework of the analysis of perturbative transport. In the cited reference, a distinction was made between the steady

state (or "power balance") transport coefficient $D^{pb} = -\Gamma/\nabla n$ (here, Γ is the particle flux and ∇n the density gradient), and the perturbation response value $D^{inc} = -\partial\Gamma/\partial\nabla n$, dubbed the "incremental" transport coefficient. If $D^{inc} > D^{pb}$, the profiles will respond sub-linearly to changes in the source term, thus producing stiffness. Accordingly, a "stiffness factor" can be defined (by analogy to [4]):

$$C = \frac{D^{inc}}{D^{pb}} = \frac{\nabla n}{\Gamma} \frac{\partial\Gamma}{\partial\nabla n}, \quad (1)$$

so that $C > 1$ would indicate some degree of stiffness.

The evaluation of D^{inc} requires a (small) perturbation of the source term and profiles, either spontaneous or induced externally. However, the relevant variables of systems near a critical steady state tend to fluctuate spontaneously around a mean value. This property can be exploited to obtain another, equivalent estimate of the stiffness that does not require perturbing the system. Interpreting the mean amplitude of the fluctuations around the steady state values (i.e. their standard deviation) as the small change symbolised by δ symbol in Eq. (1) [5]:

$$D^{fluct} = RMS(\Gamma)/RMS(\nabla n) \quad (2)$$

where $RMS(f) = \langle (f - \langle f \rangle)^2 \rangle^{1/2}$, and the angular brackets refer to a time average. In steady state, and assuming that the system response to perturbations is linear to first approximation, we expect $D^{fluct} \simeq D^{inc}$.

In the following, we study the stiffness parameter C using a simplified transport model, considered paradigmatic for transport controlled by a critical gradient. The model is described in considerable detail elsewhere [6]. The simplified model is Markovian in nature and the time evolution of the single field $n(x, t)$, which may be interpreted as a (particle) density, obeys, in one dimension, a Generalized Master Equation:

$$\frac{\partial n(x, t)}{\partial t} = S(x, t) + \frac{1}{\tau_D} \int_0^1 dx' p(x - x'; x', t) n(x', t) - \frac{n(x, t)}{\tau_D}, \quad (3)$$

The domain of the system is $0 \leq x \leq 1$, implying a normalisation of the spatial scales of the system to the system size. τ_D is a waiting time and specifies the mean time a particle remains at a given location before taking a step. We set $\tau_D = 1$, implying a normalisation of the time scales of the system to the mean waiting time. $S(x, t)$ is an external particle source, and compensates edge losses due to the absorbing boundary conditions imposed at $x = 0, 1$. The function p is a "particle step distribution". When p is Gaussian, $p(x - x', x', t) = \exp[-(x - x')^2/4\sigma^2]/2\sigma\sqrt{\pi}$, standard diffusion is recovered in the limit of small step sizes σ (and assuming a smooth density profile [7]):

$$\frac{\partial n}{\partial t} = \frac{\partial^2}{\partial x^2} \left[\frac{\sigma^2}{\tau_D} n \right] + S. \quad (4)$$

Thus, the model is closely related to standard transport models in common use.

The step distribution p is chosen as follows to produce the required critical gradient mechanism:

$$p = \begin{cases} p_0 : |\nabla n| < [\nabla n]_{\text{crit}} & \text{(sub - critical)} \\ p_1 : |\nabla n| \geq [\nabla n]_{\text{crit}} & \text{(super - critical)} \end{cases} \quad (5)$$

When the local gradient is below the critical value (sub-critical), transport is governed by the p_0 step distribution, and when it is above (super-critical), it is governed by the p_1 step distribution. Here, p_0 and p_1 are fixed and symmetric stable probability distributions (of the Lévy type, of which the Gaussian is a special case). Transport at any given location x will therefore be sub- or super-critical as a function of the local value of the density gradient. This introduces a mechanism for self-regulation into the model.

In this work, p_0 is always chosen to be a Gaussian (with width σ_0), while p_1 can either be a Gaussian (with width σ_1) or a Cauchy distribution $p_1(x - x', x', t) = \sigma_1/\pi(\sigma_1^2 + (x - x')^2)$. While a Gaussian distribution models 'normal' diffusive transport, a Cauchy distribution (with a 'long tail') is used to model processes with long-range correlations, typically called 'avalanches' or 'streamers' in the plasma transport context, and representative of turbulent or 'anomalous' transport.

To compute D^{inc} , we will be comparing steady state profiles at slightly different values of the amplitude of the source S . For simplicity, the steady state flux Γ is computed as $\Gamma(x) = \int_{0.5}^x dx' S(x')$. The lower limit of the integral corresponds to the system centre at $x = 0.5$. This calculation is sufficiently accurate for the purpose of evaluating D^{inc} . However, for the calculation of D^{fluct} we will use a different estimate of the flux that includes fluctuating contributions (see below).

The numerical calculations are performed in the domain $0 \leq x \leq 1$, on a grid with either $N = 2000$ (high resolution) or $N = 200$ (low resolution) grid points, using standard integration techniques for stiff differential equations to advance Eq. (3) in time. In all cases, the source $S(x, t) = S_0$ is taken constant. We first performed a scan of the source rate at high resolution (13 cases), and after

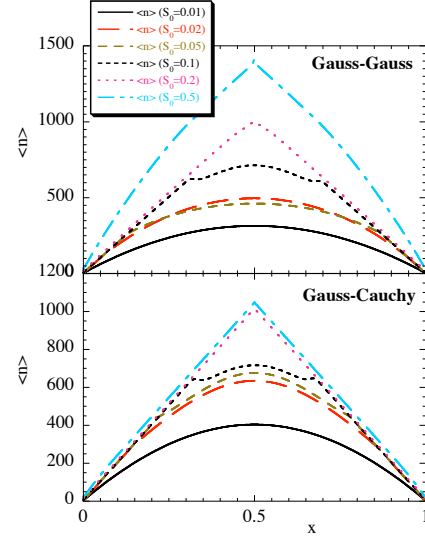


Fig. 1 Profiles vs. S_0 : Gauss-Gauss (top) and Gauss-Cauchy (bottom).

checking that the results at lower resolution were equivalent, we performed a bi-dimensional parameter scan of both the source rate and the sub-critical diffusion coefficient, the latter being proportional to σ_0^2 (130 cases).

Source scan: More details on the high-resolution calculations discussed here can be found in Ref. [8]. We set $\sigma_0 = 0.002$, while p_1 is Gaussian with $\sigma_1 = 0.008$ for the cases labelled Gauss-Gauss or "GG" (both transport channels are Gaussian), or p_1 is Cauchy with $\sigma_1 = 0.004$ for the cases labelled Gauss-Cauchy or "GC". The critical gradient is chosen $[\nabla n]_{\text{crit}} = 2000$.

For both series (GG and GC), a scan of the source rate was performed, choosing $S_0 \in \{0.01, 0.02, 0.05, 0.1, 0.2, 0.5, 10\}$. The parameter D^{inc} was computed by comparing the profiles corresponding to two subsequent values of S_0 .

Steady state profiles are shown in Fig. 1. The GG and GC profiles are very similar, except for the highest fuelling rate ($S_0 = 0.5$): whereas the GC profile remains critical across the system, the GG profile "bulges", i.e. becomes super-critical. This difference can be ascribed to the larger transport capacity of the super-critical transport channel in the GC case.

In order to quantify the stiffness, we computed the stiffness factor C . Fig. 2 shows the radial profiles of the stiffness factor C for the GC case. The spikes in the figure occur when the local values of the gradient $\nabla n(x)$ corresponding to the two subsequent values of S_0 being analysed are equal. Such points should be ignored, since their statistical error is large, and thus we will base the analysis on the global traces while ignoring the spikes. The figure shows that the critical region (where $C \gg 1$) grows from the edge inward as the source is increased. Next, a super-critical region (with $C \approx 1$) starts to grow from the edge inward. The super-critical state covers almost the whole sys-

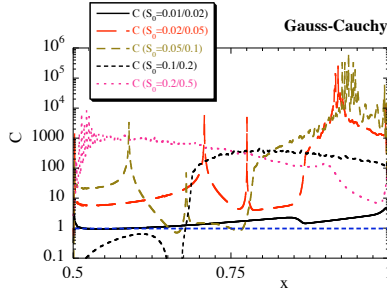


Fig. 2 Case Gauss-Cauchy: profiles of C for different combinations of the fuelling S_0 .

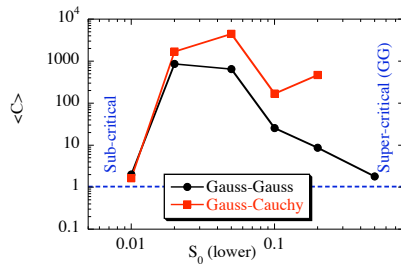


Fig. 3 Source scan, $\langle C \rangle$ vs. S_0 .

tem in the GG case at highest fuelling (not shown), while it only affects a narrow boundary layer for the highest fuelling GC case.

Fig. 3 shows $\langle C \rangle$, the radial average of C . The points in the figure are labelled by the *lower* of the two S_0 values used. In comparison to the GG cases, the GC cases do not only yield (slightly) larger values of C , but the range of values of S_0 where $C \gg 1$ exceeds the corresponding range for the GG cases.

Bi-dimensional parameter scan (source rate and diffusivity). Here we scan the source amplitude S_0 and σ_0 . The latter can be interpreted as a scan of the sub-critical diffusivity (or "collisionality"). As in Ref. [6], we set $\tau_D = 1$, $S(x) = S_0$, and $[\partial n / \partial x]_{\text{crit}} = 50$. To compute C , the same runs were repeated with $S(x) = 1.1 \cdot S_0$.

Fig. 4 shows $\langle C \rangle$ for the GG cases with $\sigma_1 = 0.08$, and for GC with $\sigma_1 = 0.04$. For GG, the largest possible value of σ_0 is σ_1 . For GC, no such limit exists on σ_0 . It is observed that $\langle C \rangle$ is a sensitive diagnostic for criticality.

In all series studied, $\langle C \rangle$ is seen to increase gradually with increasing σ_0 , reach a maximum value and then drop somewhat abruptly and make a sharp transition to its sub-critical expectation value ($C = 1$) at a precise value of σ_0 . For the GC cases, the point where the system transits from a fully sub-critical state to a critical state has been computed in previous work [6]. This critical power threshold is given by: $S_c = 2\sigma_0^2 / \tau_D [\nabla n]_{\text{crit}}$, or $\sigma_0 = \sqrt{S_c} / 10$ with our choice of parameters. This matches the results exactly.

Stiffness from fluctuations. In the case of our numer-

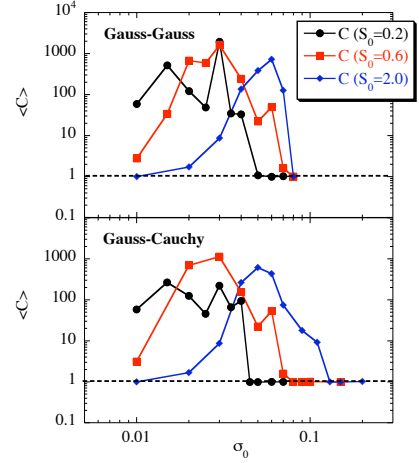


Fig. 4 $\langle C \rangle$ vs. σ_0 for various values of S_0 , cases Gauss-Gauss (top) and Gauss-Cauchy (bottom).

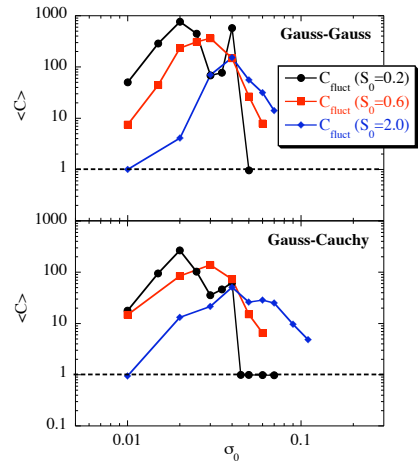


Fig. 5 $\langle C^{\text{fluct}} \rangle$ vs. σ_0 and S_0 , cases Gauss-Gauss (top) and Gauss-Cauchy (bottom).

ical model, it is straight-forward to compute the fluctuating gradient, while the flux can be evaluated from particle conservation ($\partial n / \partial t = -\partial \Gamma / \partial x + S$) in combination with Eq. (3). Thus:

$$\Gamma(x, t) = \int_0^1 dx' K(x - x', x', t) \frac{n(x', t)}{\tau_D(x')}, \quad (6)$$

where $K(x - x', x', t) = \Theta(x - x') - P(x - x', x', t)$, $\Theta(x)$ is the Heaviside function and $P(\Delta, x', t) = \int_{-\infty}^{\Delta} dx p(x, x', t)$ is the cumulative step probability distribution.

Fig. 5 shows the calculation of $\langle C^{\text{fluct}} \rangle$. Compare these results to Fig. 4. Although the maximum numerical value of $\langle C^{\text{fluct}} \rangle$ is somewhat lower than that of $\langle C \rangle$, the global trend is the same. The deviation between C and C^{fluct} at points with large stiffness is to be expected, as the system response will be strongly non-linear at such points. The calculation of C^{fluct} is not possible when the system is locally static, which explains why these figures have less data points than Fig. 4.

Heat transport. The preceding analysis was simplified by the fact that the thermodynamic force and the critical parameter were both equal to ∇n . For heat transport, these two quantities do not coincide and the definition of a stiffness quantifier is less obvious. The traditional proposal, $C = \chi^{\text{inc}}/\chi^{\text{pb}} = -\partial q/\partial(n\nabla T)/\chi$ [4], where χ is the heat diffusivity, will respond only weakly when the system criticality is not determined by $n\nabla T \simeq \text{const}$. In general, a stiffness quantifier C that responds sharply to a given critical condition should be proportional to the inverse of the change in that critical condition, as might indeed be deduced from the modelling efforts in, e.g., [9]. Since we expect Electron Temperature Gradient modes to play a role in the stiffness (if any) of the temperature profile, we believe that the critical parameter must be $\nabla T/T$ [10], so that we define the stiffness of the temperature profile by

$$C^{\text{LTe}} = \frac{1}{\chi} \frac{\partial(\chi \nabla \ln T)}{\partial(\nabla \ln T)}. \quad (7)$$

This unorthodox proposal is designed to detect the dependence of the heat diffusivity, χ , on the expected critical parameter for the ETG instability, $\nabla T/T$. Note that many alternative definitions are possible.

Application to the TJ-II Stellarator. Here we report on the first attempt to estimate the stiffness of the temperature profile in the stellarator TJ-II. Profiles at TJ-II are obtained using the single-pulse high-resolution Thomson Scattering diagnostic [11], yielding around 200 data points for the electron temperature T and density n along a chord spanning most of the plasma cross section, with a spatial resolution of 2.25 mm.

The goal of the present analysis is to determine the global transport response to a change in heating. Therefore, we fit the profiles to simple functional forms, thus ignoring any detailed radial structure. This improves the robustness of the calculation of radial derivatives needed to compute C^{LTe} . The temperature profile is fit to the sum of two Gaussians, while the density profile is fit to a Gaussian multiplied by a second-order polynomial in ρ^2 (for symmetry). $\rho = \sqrt{\psi}$ is a radial coordinate, where ψ is the normalised poloidal magnetic flux, obtained from the theoretical calculation of the magnetic flux surfaces in vacuum. Finite pressure effects can safely be ignored. The discharges studied here are those reported in Ref. [12].

The error in the profile reconstruction, evaluated using the Jacobian of the fit matrix, is of the order of 10%, lower in the centre but increasing towards the edge. While the temperature profile reconstruction is reliable (i.e. with an error less than 10%) out to about $\rho = 0.7$, the density profile reconstruction is reliable only out to about $\rho = 0.4$. The calculation of C^{LTe} is not very sensitive to the details of the density profile.

To compute χ and C^{LTe} , an estimate of the heat flux q is required. The heating source is assumed to have a Gaussian deposition profile, centred at $\rho = 0$, with a fixed width of $\Delta\rho = 0.2$. The heating efficiency is estimated to be

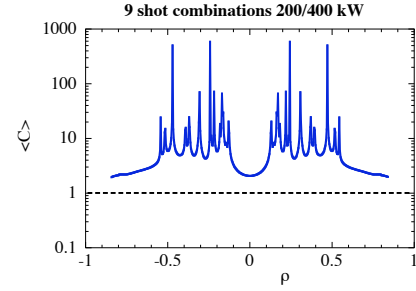


Fig. 6 Stiffness estimate for TJ-II.

60%. Radiation and other losses are ignored. The heat flux is obtained by integrating the net deposited power. In any case, the stiffness factor C^{LTe} is not very sensitive to the details of this calculation. Fig. 6 shows the mean stiffness factor, averaged over 9 equivalent discharge combinations with similar densities and different heating levels. Ignoring the spikes, one observes that a certain profile stiffness exists ($\langle C^{\text{LTe}} \rangle > 1$) in the radial range $0.15 \leq \rho \leq 0.55$, roughly coincident with the T gradient region.

Discussion. The quantification of profile stiffness is directly related to the detection of the dependence of the transport coefficient on the profile gradient. In accordance with this idea and with literature, we make use of a stiffness quantifier C , and show that it provides a useful quantification of stiffness in a paradigmatic transport model. It appears that stiffness has a radial structure and a dependence on system parameters (such as the source or drive, and the collisionality), which could possibly shed some light on the observed differences between tokamaks and stellarators.

The extension of these results to heat transport requires some care. We have suggested a definition and applied it to TJ-II data.

- [1] U. Stroth, Plasma Phys. Control. Fusion **40**, 9 (1998).
- [2] B. Carreras, IEEE Trans. Plasma Sc. **25**, 1281 (1997).
- [3] N.J. Lopes Cardozo, Plasma Phys. Control. Fusion **37**, 799 (1995).
- [4] F. Ryter, F. Leuterer, G. Pereverzev, *et al.*, Phys. Rev. Lett. **86**, 2325 (2001).
- [5] B.A. Carreras, V.E. Lynch, P.H. Diamond and M. Medvedev, Phys. Plasmas **5**, 1206 (1998).
- [6] B.Ph. van Milligen, R. Sánchez, and B.A. Carreras, Phys. Plasmas **11**, 2272 (2004) and *ibid.*, **11**, 3787 (2004).
- [7] R. Sánchez, B.Ph. van Milligen, and B.A. Carreras, Phys. Plasmas **12**, 056105 (2005).
- [8] B.Ph. van Milligen, B.A. Carreras, V.E. Lynch, and R. Sánchez, Nucl. Fusion **47**, 189 (2007).
- [9] F. Imbeaux, F. Ryter, and X. Garbet, Plasma Phys. Control. Fusion **43**, 1503 (2001).
- [10] X. Garbet, N. Dubuit, E. Asp, *et al.*, Phys. Plasmas **12**, 082511 (2005).
- [11] C.J. Barth, F.J. Pijper, H.J. van der Meiden, *et al.*, Rev. Sci. Instrum. **70**, 763 (1999).
- [12] V.I. Vargas, D. López-Bruna, J. Herranz, F. Castejón, and TJ-II Team, Nucl. Fusion, **47**, 1367 (2007).